Chapter

TiO_2 Nanoparticles Supported on Hierarchical Meso/Macroporous SiO_2 Spheres for Photocatalytic Applications

Keyla M. Fuentes, Margarita Sánchez-Dominguez and Sara A. Bilmes

Abstract

Supporting a photocatalyst, such as titania nanoparticles (TiO_2 NPs), is a good strategy to improve its performance since it can facilitate the photocatalyst recovery from the aqueous media and provides a high surface area for pollutant adsorption. Among the several advanced functional materials used as TiO_2 NP support, the hierarchical meso/macroporous SiO_2 spheres not only show the advantages associated to its chemical nature but also the dendritic fibrous structure provides a porous network that offers many benefits to be exploited in optical and catalytic devices. In this chapter, different synthetic approaches to design hierarchical meso/macroporous silica and the strategies to support TiO_2 NPs regarding the photocatalytic performance of these materials are shown.

Keywords: hierarchical SiO_2 spheres, meso/macroporous network, dendritic silica, supported TiO_2 nanoparticles, TiO_2 photocatalysis

1. Introduction

The practical applications of semiconductor photocatalysis using TiO_2 nanoparticles (TiO_2 NPs) are still limited by the catalyst recovery from the aqueous media. Supporting TiO_2 NPs on suitable materials is an advantageous strategy to overcome this issue. The effectiveness of this process requires that the supporting material has mechanical and thermal strength, high surface area for the loading of NPs, and surface sites for covalent binding to avoid NPs detachment. Nevertheless, the support must not modify the electronic structure of TiO_2 nor reduce the density of the surface defects that promotes the adsorption of reactive molecules [1–3]. Silica-based materials are attractive supports for TiO_2 due to several reasons: (i) it enhances the thermal stability of the photocatalytically active anatase phase, (ii) it avoids the particles agglomeration [4], (iii) the establishment of an Si-O-Ti interaction prevents the NPs detachment, and (iv) SiO_2 is transparent in UV-vis region and it does not interfere with the generation of electron-hole pairs in TiO_2 [5]. Additionally, SiO_2@TiO_2 core@shell structures enhance the absorption of photons due to the contrast between the refractive index producing a light-harvesting effect, which favors the photoactivity [6].

The optimal TiO_2 photocatalysts are 5–50 nm NPs in the anatase phase [7]. High loadings of NPs within this size range could be challenging for supports with low surface areas. Mesoporous silica with high surface area (500–1000 m^2/g), such as MCM-41, MCM-48, SBA-15, and KIT-6 has been widely used to deposit TiO_2 NPs [8–11]. However, the pore diameters in these materials usually range from 2 to 15 nm [12]; hence, the crystallization of NPs with sizes comparable to the pores entrances will cause, inevitably, the clogging of the pores and a significant decrease in the surface area [13].

Hierarchically porous materials have the advantage that micro- and mesopores provide the size and shape selectivity for guest molecules, enhancing the host-guest interactions, whereas macropores favor the diffusion and accessibility of guest molecules [14]. The need for tailored porous materials for different applications has motivated the design of hierarchical meso/macroporous silica by different synthetic approaches [15]; most of them are based on the sol-gel chemistry at liquid interfaces using arrangements of amphiphilic molecules as templates [16–18]. Interesting examples of these materials are the so-called dendritic fibrous nanosilicas (DFNS) [19–21], such as KCC-1 spheres (KAUST Catalysis Center-1) that are potentially useful for solving problems in catalysis, photocatalysis, DNA adsorption, CO_2 capture, optical devices, and drug delivery [22].

For photocatalytic applications, the location of the TiO_2 NPs plays an important role in the photoactivity, since NPs should be accessible for both, photons and reactive molecules. **Figure 1** illustrates the different locations of the TiO_2 NPs deposited on the fibrous silica KCC-1 in comparison with conventional mesoporous silica such as MCM-41 or SBA-15. In case of NPs deposited on KCC-1, the broad size of pore entrances facilitates the accessibility to the particles located closer to the center of the sphere.

In this chapter, we describe the synthesis pathways and the strategies for turning fibrous silica as support for photocatalytic TiO_2 NPs for applications in dye-sensitized solar cells, water splitting, and photodegradation of dyes. The advantages of using these materials as support for TiO_2 in relation to photocatalytic processes are addressed by comparing the photocatalytic activity of TiO_2 NPs deposited by different routes, as well as with TiO_2 NPs on mesoporous materials. Since the structure of these materials in the nanometer scale presents many analogies with forms of

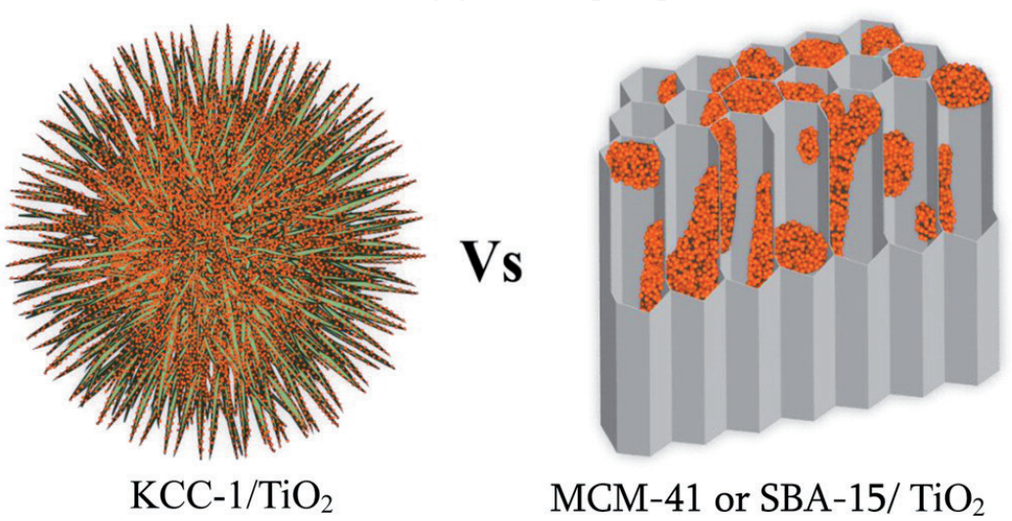

Figure 1.
Representation of TiO_2 NPs supported on fibrous nanosilica KCC-1 versus conventional mesoporous support (e.g., MCM-41 or SBA-15). The orange dots symbolize the TiO_2 NPs. Reprinted with permission from Reference [23]. Copyright 2016 American Chemical Society.

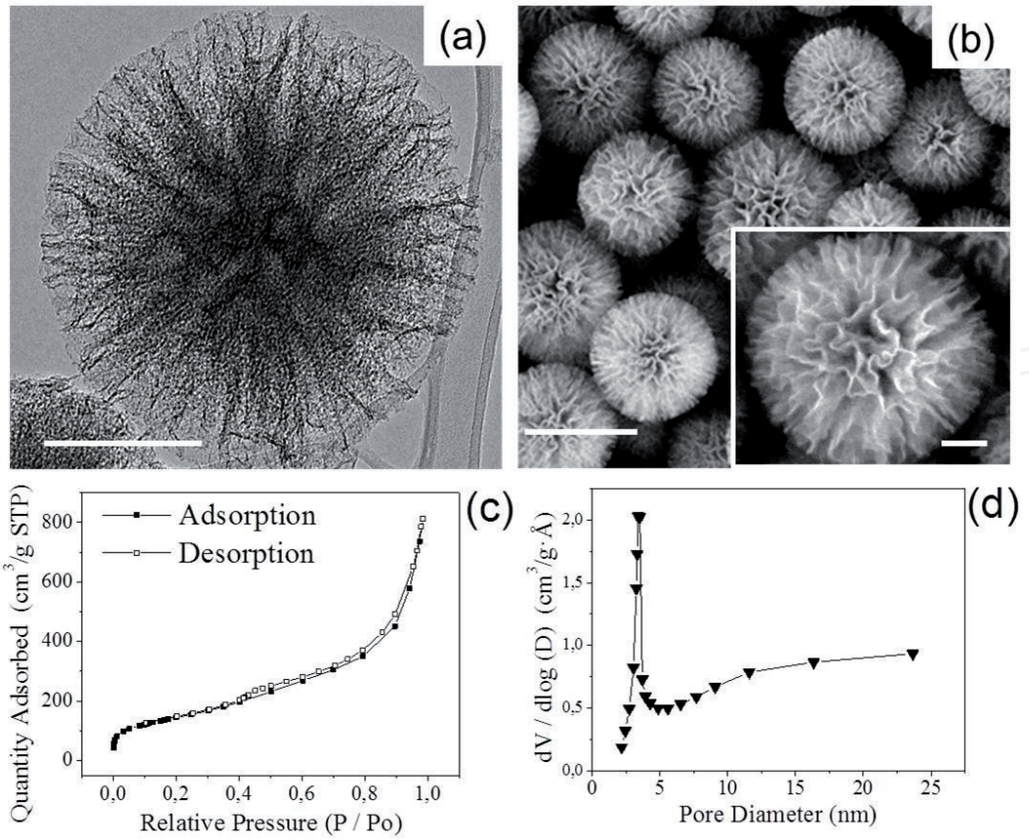

Figure 2.
TEM (a) and SEM (b) images for a representative hierarchical meso/macroporous SiO_2 spheres obtained through the synthesis by type III Winsor emulsion (see below). For the TEM image, the scale bar is 200 and 500 nm for the SEM image (scale bar of 100 nm for the inset). (c) N_2 adsorption—desorption isotherm and (d) pores size distribution (calculated by the BJH model) for the particles shown in (a and b). Unpublished results of the authors.

the micro- and macroscopic world: dendrites, carnations, wrinkles, fibers, in what follows, we will use indistinguishably the terms fibrous, dendritic, or wrinkled to refer to structures like those in **Figure 2**.

2. Synthesis of the hierarchical meso/macroporous SiO_2 spheres

Most of the novel methods for building nanostructures with tunable morphology and pore size are based on the application of an oil—water interface using amphiphilic molecules as template, which allows the preparation of materials with well-defined structures in a confined reaction media [24, 25]. By changing the oil phase, surfactant, or reaction parameters, several morphologies can be obtained, such as rod-like [26], vesicle-like [27], cage-like [28], or fibrous structures [29].

The morphological and textural characteristics of a fibrous structure are shown in **Figure 2**. Transmission electron microscopy (TEM) image reveals a darker core surrounded by a meso/macroporous shell (**Figure 2a**). Unlike the narrow pore-size distribution of common mesoporous silica materials (e.g., MCM-41 and SBA-15), these particles have radially oriented pores whose diameter increases from the center of the sphere. The scanning electron microscopy (SEM) images show a narrow distribution of particle size, and the surface of each sphere presents cavities with a broad distribution of sizes limited by folded walls (**Figure 2b**). The associated nitrogen adsorption—desorption isotherm shown in **Figure 2c** could be classified as type IV isotherm with H_3 hysteresis loop. Materials with H_3 hysteresis do not

show any limiting adsorption at high *P*/*P*o associated with nonrigid aggregates of plate-like particles and have slit-shaped pores [30]. These particles have a complex porous structure (**Figure 2d**) with pores of 3.5 nm, resulting from the surfactant assemblies that define the pore structure of the walls [31], as derived from BJH analysis of adsorption—desorption isotherms. Additionally, there is a broad distribution of larger pores related to the lamellar structure unfolding toward the particle surface.

This type of morphology with radially oriented channels can be obtained in a ternary confined reaction media composed by a surfactant and a co-surfactant, a hydrocarbon, and water. In case of particles presented in **Figure 2**, the reaction media is composed by cetyltrimethylammonium bromide (CTAB) and 1-butanol, cyclohexane, and water. Usually, the silicon sources are alkoxides, such as tetraethyl or tetramethyl orthosilicates (TEOS, TMOS) that give rise to the SiO_2 structure through sol-gel reactions.

The water-surfactant (+co-surfactant)-oil system may present one or more phases depending on the chemical composition. For instance, a thermodynamically stable microemulsion phase or multiphase systems containing a microemulsion layer can be obtained [32]. To follow the description of the formation mechanism, it is necessary to introduce some concepts related to the system.

Micelle: structures formed by self-assembly of amphiphiles in aqueous solutions giving separate regions with opposite affinities toward a given solvent. Normally, micelles have characteristic size within the 2–50 nm range and form spontaneously under certain conditions of concentration and temperature [33].

Reverse micelle: spheroidal aggregates formed by amphiphiles in organic solvents. They can be formed both in the presence and in the absence of water. In a medium free of water, the aggregates are small and polydisperse [34].

Microemulsion: system composed of water, oil, and an amphiphile, which is a single optically, isotropic, and thermodynamically stable liquid solution [35]. The microemulsions can exist as oil-swollen direct micelles dispersed in water (O/W microemulsions), water-swollen reverse micelles dispersed in oil (W/O microemulsions), or with both aqueous and oily continuous domains as interconnected sponge-like channels (bicontinuous microemulsions) [36].

Winsor emulsion systems: the Winsor classification of ternary systems, i.e., types I–IV, can be made according to the numbers and type of phases in the equilibrium state. Except for the single-phase microemulsion (type IV), the structure of the microemulsion is determined through the separation of the solvent from the dispersed phase of the microemulsion layer. Type I: at equilibrium, superfluous oil separates from the oil-in-water microemulsion. Type II: superfluous water separated from the microemulsion layer. Type III: both superfluous oil and water separated from the water-in-oil microemulsion [32].

Mesophase: a phase occurring over a defined range of temperature, pressure, or composition within the mesomorphic state. This is a state of matter in which the degree of molecular order is intermediate between the three-dimensional, long-range order found in solid crystals and the order found in isotropic liquids, gases, and amorphous solids [37].

Sol-gel reactions: these are kinetically controlled hydrolysis and polycondensation reactions of a metallic precursor (e.g., inorganic or alkoxide), which give rise to a metal oxide structure. The precursor, building blocks, evolves in several steps from dispersions of colloidal particles in a liquid (Sol) to interconnected polymeric chains forming a porous rigid network (gel) [38]. The most generally accepted model to describe silica polymerization in aqueous media is nucleation and growth [39].

2.1 Proposed mechanism for the formation of the hierarchical porous SiO_2 using oil-in-water emulsions

The general mechanism for the formation of hierarchical porous silica using oil-in-water emulsion made from a type III Winsor system can be described in the following steps, also schematized in **Figure 3** [20]:

1. The silicon source dissolved in the oil layer meets the water layer—an aqueous solution of a base—at the emulsion interface; the sol-gel reactions take place at this stage. In the basic solution, the reaction mixture contains ionized silicate monomers and oligomers negatively charged. As the silica condensation proceeds, the amount of partially condensed silicates decreases and that of fully condensed silicates increases.

2. Silicate oligomers interact with the surfactant heads giving rise to a change in the curvature of the interface.

3. As the curvature increases, a closed structure such as spherical or cylindrical shapes can be formed. These surfactant-silicate systems with closed structure lead to the formation of micelles or micellar emulsions inside the channels of the bicontinuous microemulsion.

4. The aggregation of these micelles leads to the formation of a repetitive mesophase.

However, in this mechanism, the growth of the particle is still unclear. It can be thought that the formed mesophase may act as a seeding site were the wrinkles grow through the water channels. As particles start growing, the structure of the microemulsion is rearranged, and according to Moon and Lee [20], the walls of wrinkles are formed in the water layers and the valleys are consequences of the oil phase in the microemulsion.

An alternative mechanism was proposed by Febriyanti et al. [40], considering the optimal conditions for the synthesis of KCC-1 [29]. They suggest the formation of reverse micelles in which the sol-gel reactions take place at higher rate in the center of the droplet. This mechanism is schematized in **Figure 4**. Although this mechanism explains the TEM images in which the density of the particles seems to decrease from the center to the surface of the sphere, experiments using real-time small angle X-ray scattering and 3D tomography demonstrate that the fibers grow uniformly from the

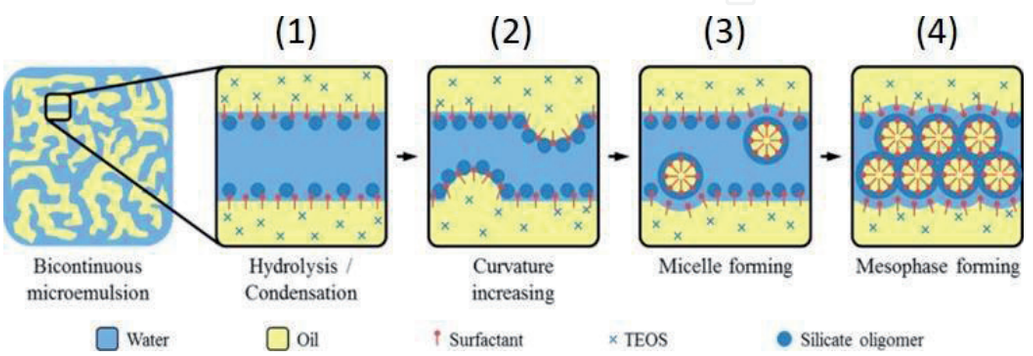

Figure 3.
Schematic illustration of the mesophase-forming mechanism from the microemulsion interface. Reprinted with permission from Reference [20]. Copyright 2012 American Chemical Society.

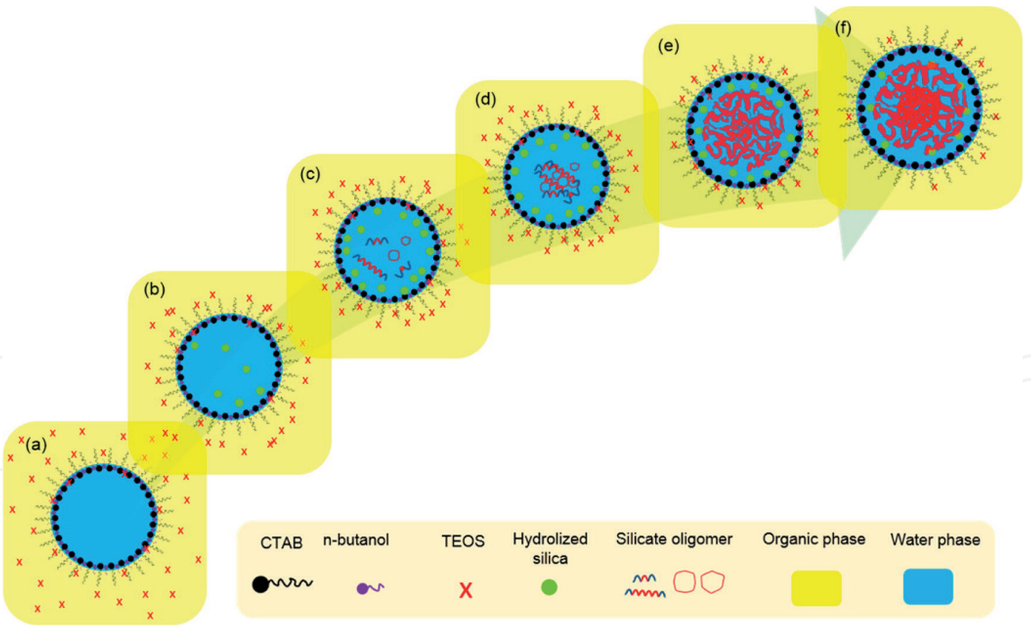

Figure 4.
Schematic representation of the KCC-1 synthesis in the reverse emulsion system proposed by Febriyanti et al. Reprinted with permission from Reference [36]. Copyright © 2016, American Chemical Society.

center of the spheres along the free radial directions to form fibrous spherical silica particles. Based on these results, Maity et al. [41] described the microemulsion-droplet-coalescence mechanism.

2.2 Tuning the morphology and pore size distribution of the hierarchical meso/macroporous silica spheres

The possibility to obtain tailor-made supports for specific guest molecules and tunable pore volume for loading control is the most attractive feature of the three-phase synthesis approach. In case of fibrous nanosilica KKC-1, the surface area may vary from 450 to 1244 m^2/g, and the tunable pore sizes (3.7–25 nm) allow to increase the pore volume up to 2.18 cm^3/g. Likewise, the particle size can be controlled from 40 to 1120 nm. [42]. Parameters controlling particle size, pore volume, and surface area are discussed below.

2.2.1 Oil phase

Shen et al. developed a stratification approach to obtain a three-generation pore size by changing the oil phase in a biphasic system [43]. They used 1-octadecene, decahydronaphthalene (decalin), and cyclohexane to pores of sizes 2.8, 5.5, and 7.0 nm in the same particle. Each mesoporous shell was obtained in a synthesis step using the corresponding oil phase. This confirms that the organic solvent not only provides a storage medium for the silicon source (TEOS), but also interacts and assembles with the surfactant molecules in the interface to form oil-in-water microemulsion droplets. **Figure 5** shows the dendritic particles obtained by the biphasic stratification approach.

2.2.2 Surfactant

Depending on the molar ratio of surfactant to silicon, the surfactant participates in the synthesis with different functional roles: controlling the particle diameter, the particle dispersion in the medium, and the degree of mesophase formation.

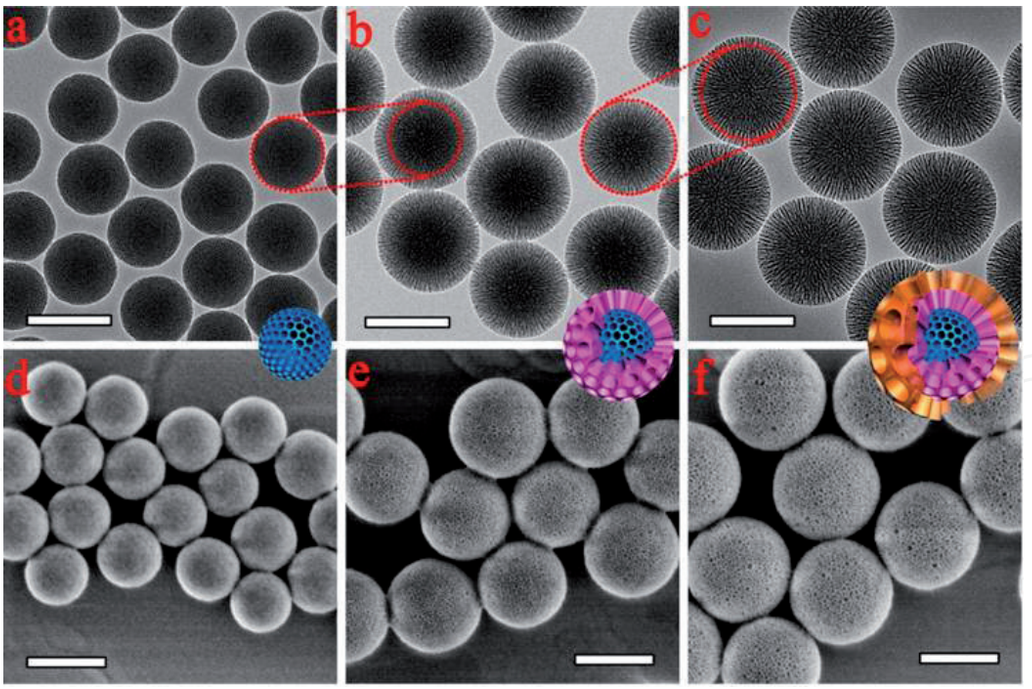

Figure 5.
TEM (a-c) and SEM (d-f) images of the extracted 3D-dendritic MSNSs with one (a and d), two (b and e), and three generations (c and f) prepared via the biphase stratification approach. All scale bars in TEM and SEM images are 200 nm.

As the surfactants favor the dispersion of the alkoxysilanes in water, the hydrolysis reactions are favored in comparison with the condensation reactions leading to an increased nucleation rate. The net effect is that increasing the surf/Si ratio, the particle diameter decreases. Moreover, at a high surf/Si ratio, free micelles may adsorb in the primary particles, allowing the dispersion of the particles due to electrostatic and/or steric repulsion. In contrast, at low surf/Si ratios, the surfactants mainly act as porogen [44]. For the KCC-1 synthesis using benzyldimethylhexadecyl ammonium chloride (16- BAC) instead of CTAB, the fibrous morphology is lost due to the differences in the packing parameters, which in turn depend on the length of the nonpolar chain and the effective area of the polar head [29].

2.2.3 Co-surfactant

By increasing the alkyl chain length of the co-surfactant (linear C_3-C_{20} alcohols), the distance between wrinkle walls increases, as shown in **Figure 6**. As the affinity between oil and surfactant defines the valleys of the wrinkles, an increase in the hydrophobicity of the aqueous phase by enlarging the co-surfactant alkyl-chain broadens the distance between the wrinkle walls. It can be considered that this distance is directly related to the density of fibers by changing this parameter, the pore size distribution in the region related to the lamellar structure and the pore volume also changes, but the surface area remains unaltered [20].

2.2.4 Composition of the water phase

The type and concentration of the base catalyst dissolved in the aqueous phase affects the diameter of the spheres, as it controls the hydrolysis rate of the silicon source. Due to their buffer capacity, weak bases are preferred. For instance, basic amino acids, such as arginine or lysine, keep the reaction under weakly basic conditions leading to spherical particles with dendritic pores [18, 45]. The same particles

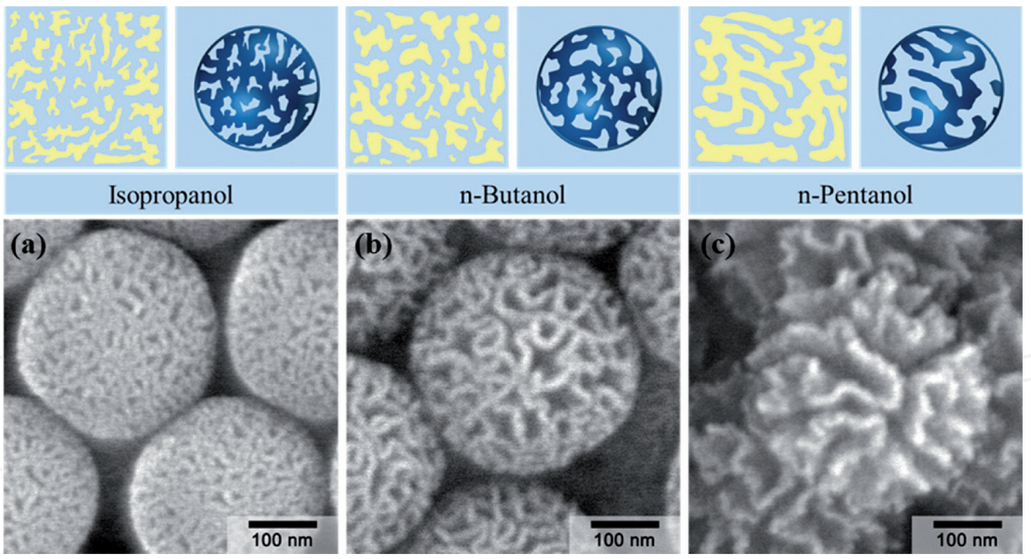

Figure 6.
Schematic illustrations of microemulsion phases of reaction mixtures with different co-solvents (6.0 mmol) and corresponding SEM images of the resulting wrinkled SiO_2 spheres: (a) isopropanol, (b) n-butanol, and (c) n-pentanol. Reprinted with permission from Reference [20]. Copyright 2012 American Chemical Society.

can be obtained with urea, whose thermal decomposition above 70°C maintains the solution pH between 7 and 9.5, depending on the urea concentration [46]. Nevertheless, the increase in urea concentration rises the nucleation rate leading to smaller particles.

2.2.5 Stirring

Jin et al. [47] found that keeping constant the emulsion composition to obtain rod-like structures at low stirring speeds (i.e., <300 rpm) produces twisted-ribbon or twisted-rod-like structures with changes in the length and the diameter of the rods. On the other side, high stirring speeds (i.e., 1200 rpm) yield spherical or irregular morphologies. The stirring speed has two main effects in the synthesis: (i) it alters the self-assembly of the template and (ii) it affects the diffusion of the reagents to the interface [17]. In the synthesis of wrinkled SiO_2, high stirring speeds (around 900 rpm) are preferred to obtain a spherical morphology.

2.2.6 Reaction time

Hydrolysis and condensation rates for silica at pH 7–9 are slow processes occurring simultaneously with changes in surfactant assemblies. The synthesis of dendritic particles in the conditions giving the product as depicted in **Figure 2** requires around 20 h to be completed. The particle evolution during these conditions monitored by SEM is shown in **Figure 7**. After 4 h, slightly structured particles (≤100 nm) are formed. As the reaction proceeds, lamellae are defined and particles grow, reaching an average diameter of 300 nm with high size dispersion after 6 h. Once lamellae are formed, the effect of reaction time is a slow increase of particle size up to 500 nm in 24 h, less polydispersion, and well-defined planes of wrinkles with deep valleys.

Several processes converge to achieve these corrugated particles. On the one hand, the silicon precursor condenses on the already formed silica units. On the other hand, there is a simultaneous silicate dissolution and re-precipitation (Oswald ripening) that generates hydrophilic silica surfaces. This process induces the formation of hydrophobic regions where the organic phase is accumulated giving

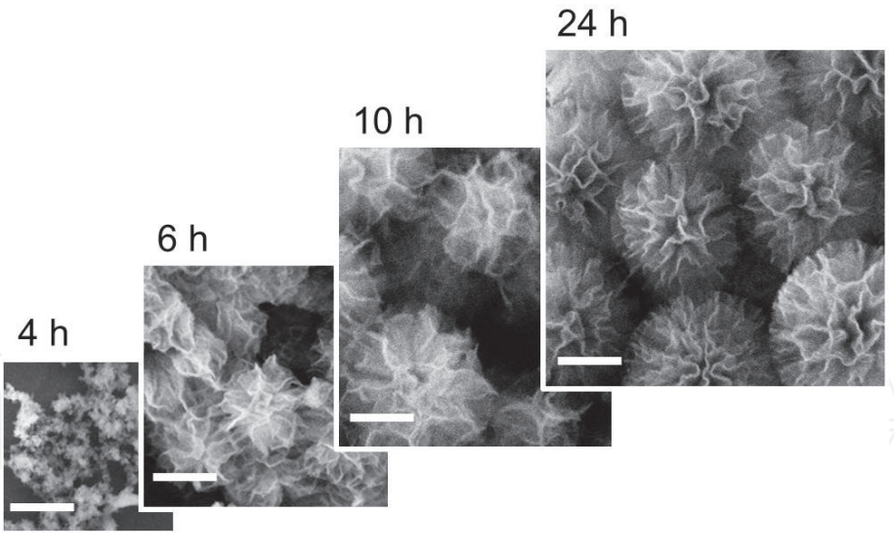

Figure 7.
Evolution of the growth in time of the particles shown in ***Figure 2*** *monitored by SEM. Scale bars are 200 nm. Unpublished result from authors.*

rise to the deep valleys observed for 24 h. Although data on the kinetics of dendritic particles formation are scarce, it is known that the reaction may be accelerated by the assistance of microwave radiation, as proposed for the synthesis of the KCC-1. Under these conditions, particles are formed in few minutes but for longer reaction times (>60 min); the lamellae collapse producing denser particles [42]. This experiment reinforces the idea that the necessary condition for having a dendritic structure is the formation of hydrophobic "pockets," a process that is inhibited when microwave radiation is applied.

In summary, the main advantage of the synthesis using oil-in-water Winsor III emulsion is the production of dendritic particles that can be tailored by the synthesis parameters for a specific need. The adjustment of pore sizes is important for trapping biomolecules or nanoparticles and for diverse catalytic applications that require high surface area and pore volume. Moreover, for environmental applications, the particle size is a key factor for catalyst recovery. The surfactant to Si ratio and the concentration of the base catalyst are important parameters for controlling the particle diameter, whereas the microemulsion phase behavior defines the distance between the wrinkle walls, i.e., the macroporosity. For a given surfactant, the microemulsion structure is affected by the organic solvent and the co-surfactant chain length, which will tailor the size of cavities and fiber density. The reaction time is an empiric variable for each reaction set-up, which needs to be optimized to get the required product.

3. Strategies for supporting TiO_2 NPs on hierarchical meso/macroporous silica spheres and photocatalytic performance

Catalysts based on Ti-containing mesoporous silica, e.g., MCM-41. SBA-15 has been developed from different synthetic pathways for applications such as selective oxidation of bulky organic compounds and photoreduction of greenhouse gases [48, 49].

Typically, two synthesis strategies could be applied depending on the stage of incorporation of the TiO_2 precursor: (i) *one-pot*: added directly to the SiO_2 reaction mixture (co-condensation route) or (ii) *postsynthesis*: added after the consolidation of the SiO_2 network by deposition, impregnation, atomic layer deposition, among

others. In the one-pot approach, the co-condensation of titanium precursor with the silicon source faces with the problem that Ti alkoxides are much more reactive than $Si(OR)_4$ [50]; thus, it is necessary to control the Ti precursor hydrolysis in order to have an appropriate distribution of Ti species that lead to the formation of anatase nanocrystals, a necessary component for efficient photocatalysis [51].

In this section, we focus on different postsynthesis pathways leading to photocatalytic systems for energy conversion, H_2 production, or photodegradation of dyes. The consolidated SiO_2 porous network must ensure high loadings of homogeneously distributed TiO_2 NPs attached by covalent interactions, while the deposition method determines the location and structure of the nanoparticles, e.g., particle size and crystallinity. All these features affect the photocatalytic performance of the semiconductor.

TiO_2 NPs deposited on KCC-1 by atomic layer deposition (ALD) alternating titanium tetra-butoxide and hydrogen peroxide produces anatase NPs of 3–12 nm highly dispersed on the fibers (**Figure 8a**) whose diameter increases with the number of ALD cycles [21]. The anatase phase was obtained after the ALD cycles by calcination at 300–700°C. This material exhibits high photocatalytic activity and turnover frequency (TOF) towards the Rhodamine B (Rh-B) photodegradation under UV light, even better than the one obtained using the same ALD procedure with MCM-41 and SBA-15 substrates (**Figure 8b** and **c**). This higher photoactivity may be a consequence of the location and distribution of TiO_2 NPs on the support allowing an optimal dye-TiO_2 interaction for a hole transfer or improved OH• attack

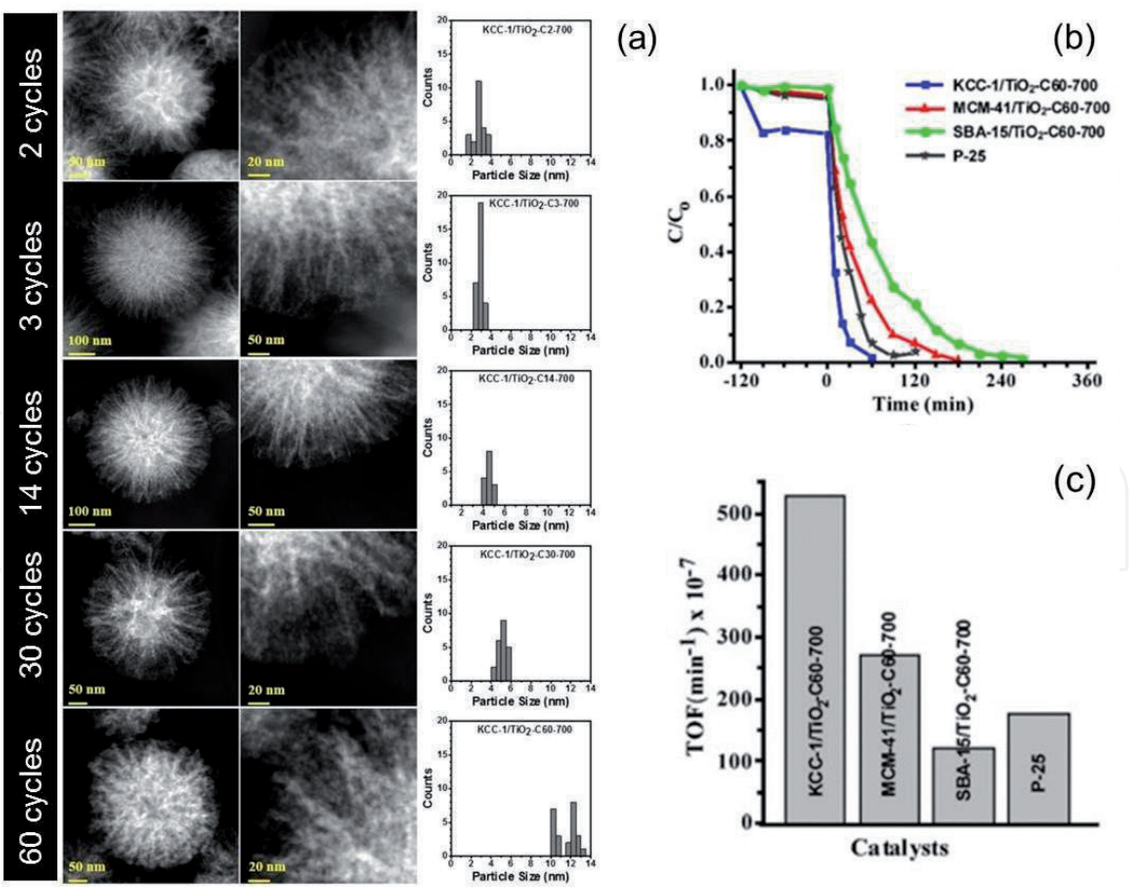

Figure 8.
(a) Scanning transmission electron microscopic images (STEM) of KCC-1/TiO_2 after several ALD cycles and heat treatment at 700°C, the corresponding histogram for the average particle size is showed next to each image. (b) Photocatalytic degradation of rhodamine B using KKC-1/TiO_2 compared to equivalent catalyst using common mesoporous silica and a commercial Degussa P25. (c) Turnover frequency (TOF) for the reaction: it was estimated as the moles of dye degraded per mole of TiO_2 per minute. Adapted from Reference [23]. Copyright 2016 American Chemical Society.

to the dye. The open structure of the fibrous silica admits higher TiO_2 loading accessible to the dye, while the ordered array of mesoporous channels in MCM-41 and SBA-15 is easily clogged by TiO_2 NPs as schematized in **Figure 1**. The TiO_2 loading on SiO_2 is determined by the surface silanol/siloxane ratio which is independent on synthesis method [52]. Thus, even all substrates exhibit nearly the same TiO_2 loading in weight (**Figure 9**), the more open structure of KCC-1 allow better accessibility to Ti precursors as ALD cycles increase.

Enhanced photocatalytic activity can also be explained by higher photon harvesting in the fibrous structure of the KCC-1 [42], as these structures enable incident light to pass through the cavities and reduce optical loss due to multiple light scattering and reflection [53]. The efficient photon harvesting of dendritic particles was also exploited for the design of dye-sensitized solar cells (DSCs) [48]. By modifying the interwrinkle distances in the silica spheres with the co-surfactant's length of the carbon chain, the fiber density changes from narrow (NWSNs) to wide (WWSNs) wrinkled silica. In this case, TiO_2 NPs were deposited by dispersing the SiO_2 spheres in a mixture of acetonitrile- ethanol (1:1) using ammonia solution to conduct the hydrolysis/condensation reactions of titanium ter-butoxide. Using this approach, 4 nm anatase crystallites were obtained after calcination at 500°C under air atmosphere. The dependence of photovoltaic parameters with the fiber density is interpreted as a consequence of the effective refractive index resulting from the combination of two materials with different optical properties, supporting the idea of improved photon harvesting promoted by the fibrous nature of the SiO_2 spheres.

In the latter cases, the crystallization of TiO_2 was conducted by calcination at temperatures higher than 300°C. Despite the fact that porous silica spheres have good thermal stability, the calcination presents several drawbacks for the photocatalytic process: (i) it reduces the surface hydroxyl groups and surface area [54] and (ii) it induces the anatase to rutile transformation leading to a decrease in photoactivity [55]. Although anatase-rutile phase transition can be managed with the calcination temperature and by the introduction of defects, hydrothermal synthesis of TiO_2 NPs is a more convenient method for producing anatase nanocrystals on silica substrate [6].

On the hydrothermal route, the solvent has a strong impact on the TiO_2 NP size and distribution [56]. Under soft conditions (180°C, 20 h) in ethanol-water mixtures, the TiO_2 NPs are homogeneously located in the outermost zone of KCC-1 particles when using pure water. This causes an increment in the specific surface area and pore volume; whereas, by using absolute ethanol, the particles are dispersed in the fibers (see TEM images and particle size distribution in **Figure 10a**). Regarding

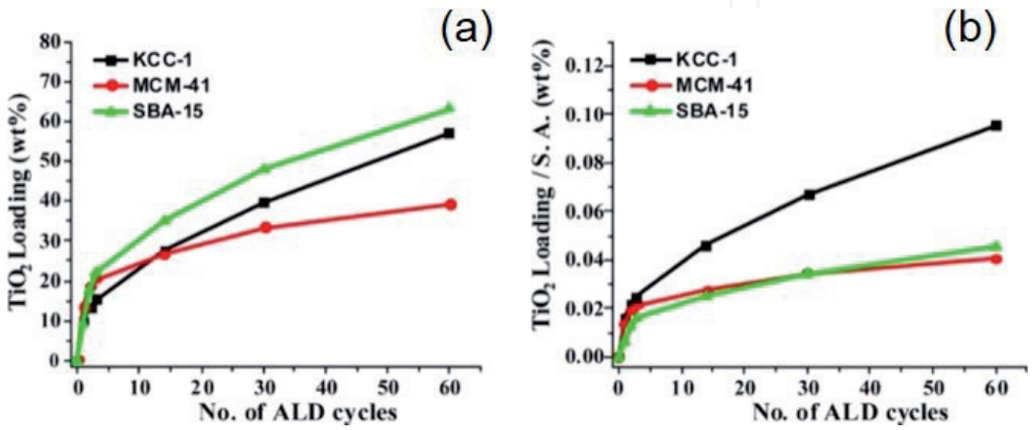

Figure 9.
TiO_2 loading on KCC-1, MCM-41, and SBA-15 deposited by ALD. The loading is expressed as wt% (a) and wt% per unit surface area (b). Reprinted from Reference [23]. Copyright 2016 American Chemical Society.

the TiO_2 NPs sizes, it goes from 8 nm to 17.5 nm by increasing the ethanol/water ratio from 0/100 to 28.5/1.5. Then, it decreases to 5 nm in a 100/0 ratio; under this condition, a narrower size distribution is obtained. As far as photocatalytic activity is concerned, particles prepared with absolute ethanol showed the highest activity for water splitting under UV light (**Figure 10b**). This result points out that the size and location of the TiO_2 NPs plays a significant role in the photocatalytic performance. The TiO_2 NP distribution leads to different morphologies with a characteristic effective refractive index, which defines the interaction with the incident photons. Thus, by controlling the accessibility of the TiO_2 NPs to the porous system, it is possible to design suitable morphologies for improving photocatalysis.

Another alternative to control the TiO_2 NP location is by taking advantage of the reagents used during the synthesis of the support. As shown in the previous section, the synthesis of wrinkled SiO_2 spheres (see **Figure 2**) requires high amounts of CTAB acting as a pore template. Thus, it is possible to imagine that before removing the template, the pores are "filled" with CTAB molecules blocking the transport of Ti precursors. On this basis, our group developed a practical approach to handle the TiO_2 NP distribution on wrinkled SiO_2 spheres (460 nm in diameter, B.E.T. area = 550 m^2/g) produced by hydrothermal synthesis using Ti isopropoxide in isopropanol. With this hydrothermal synthesis, TiO_2 NPs of 10 nm with 6-nm anatase crystallites are obtained. The loading and location of the NPs significantly differ depending on the presence of CTAB during the hydrothermal treatment. **Figure 11a** summarizes the experimental approach for controlling the TiO_2 NP location and their corresponding TEM and SEM images (**Figure 11b**). In **Figure 11**, *w*-SiO_2@TiO_2 refers to NPs deposited after the removal of CATB and w-SiO_2/CTAB@TiO_2 to NPs deposited in the spheres containing CTAB. By eliminating CTAB prior to TiO_2 deposition, NPs are highly dispersed in a hybrid SiO_2-TiO_2 shell, resulting in a greater decrease in surface area than when TiO_2 NP growth is performed in the presence of CTAB. This morphology resembles that

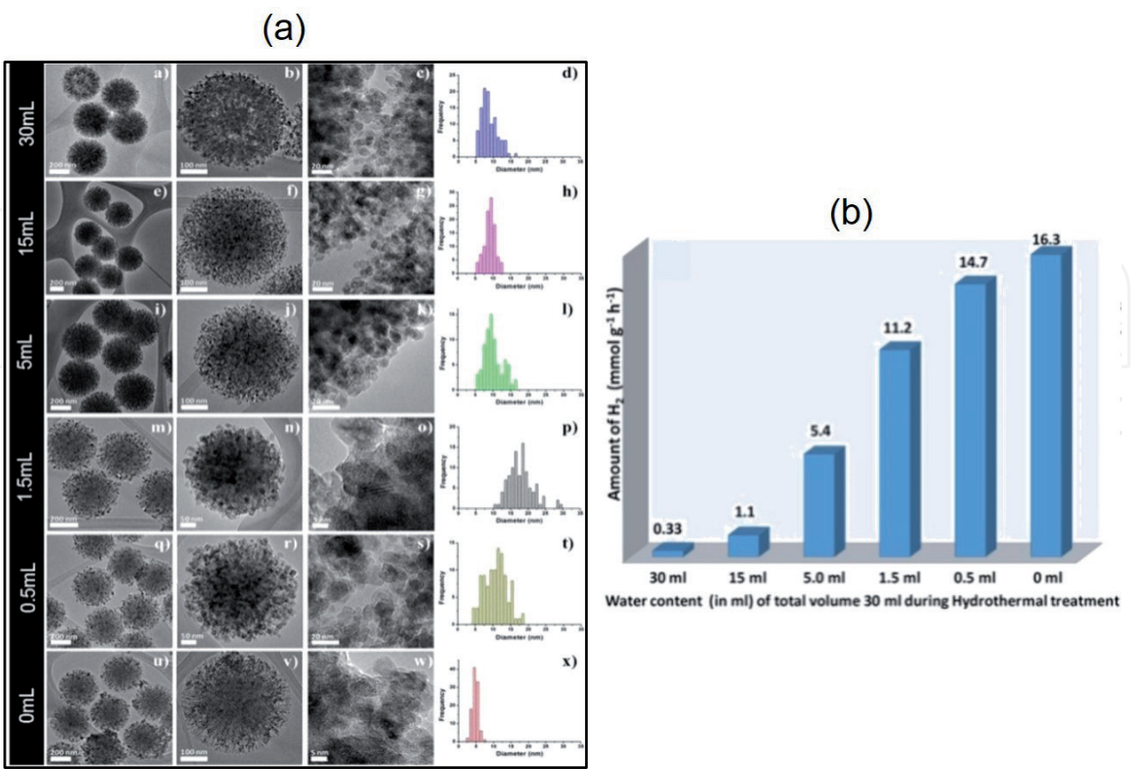

Figure 10.
(a) TEM images in three magnifications and corresponding histograms for the particle size distribution after hydrothermal treatment at 180°C obtained in varying water content (inset: a-x). (b) H_2 evolution using the samples showed in the SEM images [56].

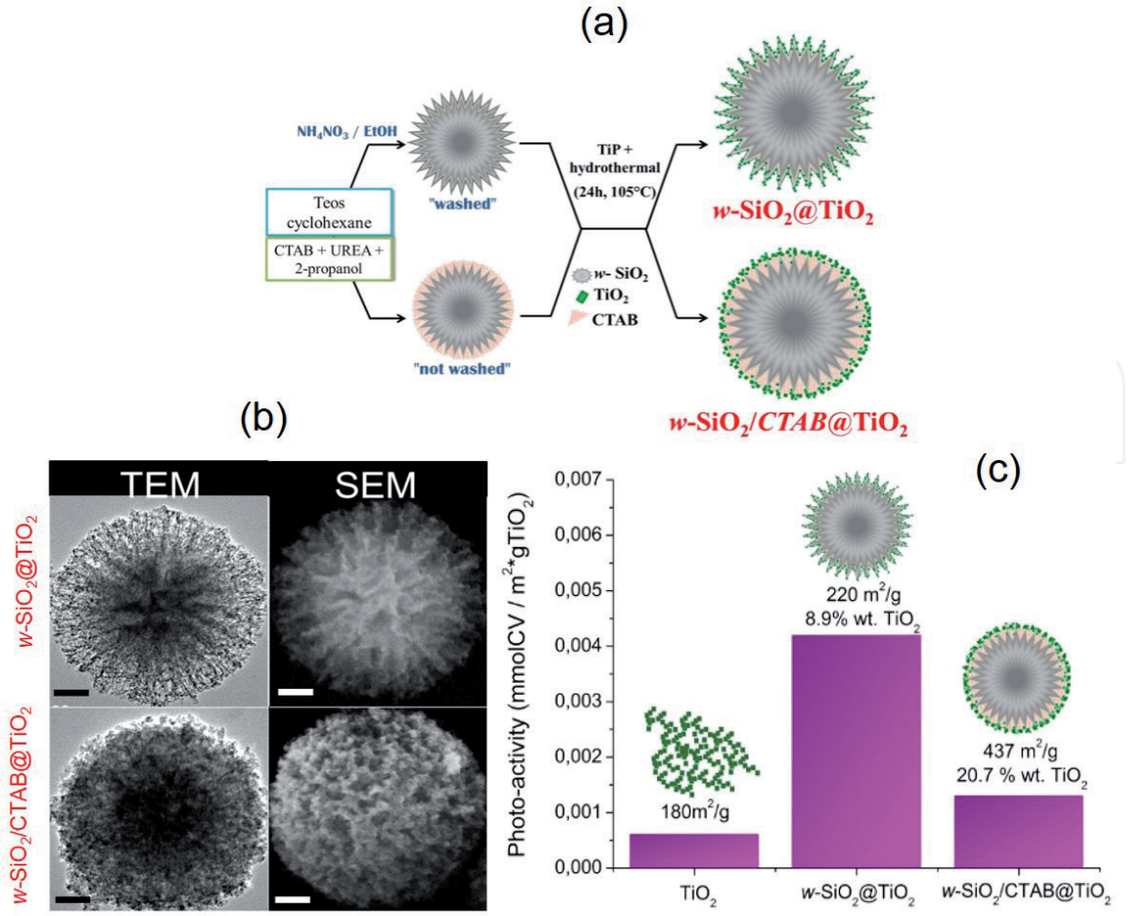

Figure 11.
(a) Experimental scheme for the synthesis of wrinkled-SiO_2@TiO_2 particles, (b) corresponding TEM and SEM images, the scale bar are 100 nm, and (c) photoactivity of the wrinkled-SiO_2@TiO_2 particles in comparison with the unsupported TiO_2 NPs. Unpublished results of the authors.

obtained by atomic layer deposition (ALD) [21], as shown in **Figure 8a**. On the other side, when the hydrothermal process is carried out in the presence of CTAB, the NPs are arranged as a mesoporous TiO_2 layer in the same way as the particles obtained by hydrothermal crystallization described in **Figure 10a** [51]. Therefore, this synthetic approach provides different morphologies simply by taking advantage of CTAB molecules from the synthesis of SiO_2 particles. The photoactivity of these particles was tested in the degradation of crystal violet (CV). As seen in **Figure 11c**, CV photodegradation occurs at higher rate when using SiO_2-TiO_2 hybrid layer particles (w-SiO_2@TiO_2) whose morphology allows better photon harvesting. In case of w-SiO_2@CTAB TiO_2 particles, the presence of CTAB increases the adsorption of the dye, thus providing a basis to functionalize the SiO_2 particles for a more specific interaction with the targets. Finally, the dimensions of the support are adequate for a good recovery of the reaction medium providing an efficient system for environmental applications.

4. Summary and outlook

Meso/macroporous silica spheres are remarkable supports for TiO_2 NPs as compared to conventional silica mesoporous materials, such as MCM-41 and SBA-15. The main advantage of this morphology is the accessibility of the molecules to the silica surface provided by the broad pore size distribution. For photocatalytic applications, the location of TiO_2 nanoparticles is a critical parameter to optimize the photoactivity. Supported TiO_2 NPs in these materials exhibit:

i. better accessibility to the active sites ensuring high TiO_2 loadings;

ii. high surface area, which favors higher adsorption of the pollutants;

iii. enhanced photocatalytic performance for several target molecules;

iv. improved light harvesting; and

v. facile recovery from the reaction media compared to unsupported TiO_2 NPs.

The easy tailoring of the surface properties provides photocatalysts for specific applications that can be rationalized by considering the location of TiO_2 NPs on the porous support, which in turn can be managed by the synthesis variables. Understanding the internal nature of the hierarchical supports of the photoactive TiO_2 allows the development of value in photocatalysis for energy and environmental applications—a contribution of material's scientists to a better world.

Acknowledgements

The authors are grateful with CONICET for the postdoctoral scholarship of K.M.F., and University of Buenos Aires for funding, UBACyT 20020170200298BA. We are in indebted to Nanoandes Network and ERANET-LAC FP7 project Recola for the continuous support. Also, we acknowledge Stefanie Kodjikian (Institut NÉEl, Grenoble) and Maria Claudia Marchi (CMA-CONICET) for TEM and SEM images, respectively.

Conflict of interest

There are no conflict of interest to declare.

DOI: http://dx.doi.org/10.5772/intechopen.86153

Author details

Keyla M. Fuentes[1,2*], Margarita Sánchez-Dominguez[2] and Sara A. Bilmes[1]

1 Instituto de Química Física de los Materiales, Medio Ambiente y Energía-(INQUIMAE-CONICET), Departamento de Química Inorgánica, Analítica y Química Física (DQIAQF), Facultad de Ciencias Exactas y Naturales, Universidad de Buenos Aires, Ciudad Universitaria (C1428EHA), Ciudad Autónoma de, Buenos Aires, Argentina

2 Centro de Investigación en Materiales Avanzados, S.C. (CIMAV), Apodaca, Nuevo León, México

*Address all correspondence to: keylafuentesflores@gmail.com

References

[1] Miar Alipour S, Friedmann D, Scott J, Amal R. TiO_2/porous adsorbents: Recent advances and novel applications. Journal of Hazardous Materials. 2018;**341**:404-423. DOI: 10.1016/j.jhazmat.2017.07.070

[2] Schneider J, Matsuoka M, Takeuchi M, Zhang J, Horiuchi Y, Anpo M, et al. Understanding TiO_2 photocatalysis: Mechanisms and materials. Chemical Reviews. 2014;**114**:9919-9986. DOI: 10.1021/cr5001892

[3] Regazzoni AE, Mandelbaum P, Matsuyoshi M, Schiller S, Bilmes SA, Blesa MA. Adsorption and photooxidation of salicylic acid on titanium dioxide: A surface complexation description. Langmuir. 1998;**14**:868-874. DOI: 10.1021/la970665n

[4] Lee D-W, Park S-J, Ihm S-K, Lee K-H. Synthesis of bimodal mesoporous titania with high thermal stability via replication of citric acid-templated mesoporous silica. Chemistry of Materials. 2007;**19**:937-941. DOI: 10.1021/cm062465f

[5] Fuentes KM, Betancourt P, Marrero S, García S. Photocatalytic degradation of phenol using doped titania supported on photonic SiO_2 spheres. Reaction Kinetics, Mechanisms and Catalysis. 2017;**120**:403-415. DOI:10.1007/s11144-016-1097-3

[6] Ullah S, Ferreira-Neto EP, Pasa AA, Alcântara CCJ, Acuña JJS, Bilmes SA, et al. Enhanced photocatalytic properties of core@shell SiO_2@TiO_2 nanoparticles. Applied Catalysis B: Environmental. 2015;**179**:333-343. DOI: 10.1016/j.apcatb.2015.05.036

[7] Chen J, Qiu F, Xu W, Cao S, Zhu H. Recent progress in enhancing photocatalytic efficiency of TiO_2-based materials. Applied Catalysis A: General. 2015;**495**:131-140. DOI: 10.1016/j.apcata.2015.02.013

[8] Zhang F, Zheng Y, Cao Y, Chen C, Zhan Y, Lin X, et al. Ordered mesoporous Ag–TiO_2–KIT-6 heterostructure: Synthesis, characterization and photocatalysis. Journal of Materials Chemistry. 2009;**19**:2771. DOI: 10.1039/b818495j

[9] Li Y, Li N, Tu J, Li X, Wang B, Chi Y, et al. TiO_2 supported on rod-like mesoporous silica SBA-15: Preparation, characterization and photocatalytic behaviour. Materials Research Bulletin. 2011;**46**:2317-2322. DOI: 10.1016/j.materresbull.2011.08.044

[10] Tian L, Liu H, Gao Y. Degradation and adsorption of rhodamine B and phenol on TiO_2/MCM-41. Kinetics and Catalysis. 2012;**53**:554-559. DOI: 10.1134/S0023158412050175

[11] Mureseanu M, Parvulescu V, Radu T, Filip M, Carja G. Mesoporous CeTiSiMCM-48 as novel photocatalyst for degradation of organic compounds. Journal of Alloys and Compounds. 2015;**648**:864-873. DOI: 10.1016/j.jallcom.2015.07.078

[12] Garg S, Narayan R, Nayak UY, Raichur AM. Mesoporous silica nanoparticles: A comprehensive review on synthesis and recent advances. Pharmaceutics. 2018;**10**:1-50. DOI: 10.3390/pharmaceutics10030118

[13] Fei X, Dong Y, Liu Y. Study on synthesis and properties of composite mesoporous TiO_2/MCM-41 photocatalysts. Materials and Technologies. 2016;**31**:423-429. DOI: 10.1179/1753555715Y.0000000073

[14] Su B-L, Sanchez C, Yang X-Y, editors. Hierarchically Structured Porous Materials. Weinheim, Germany: Wiley-VCH Verlag GmbH & Co. KGaA; 2011. DOI: 10.1002/9783527639588

[15] Sun M-H, Huang S-Z, Chen L-H, Li Y, Yang X-Y, Yuan Z-Y, et al. Applications of hierarchically structured porous materials from energy storage and conversion, catalysis, photocatalysis, adsorption, separation, and sensing to biomedicine. Chemical Society Reviews. 2016;**45**:3479-3563. DOI: 10.1039/C6CS00135A

[16] Yokoi T, Karouji T, Ohta S, Kondo JN, Tatsumi T. Synthesis of mesoporous silica nanospheres promoted by basic amino acids and their catalytic application. Chemistry of Materials. 2010;**22**:3900-3908. DOI: 10.1021/cm9037846

[17] Sun B, Zhou G, Zhang H. Synthesis, functionalization, and applications of morphology-controllable silica-based nanostructures: A review. Progress in Solid State Chemistry. 2016;**44**:1-19. DOI: 10.1016/j.progsolidstchem.2016.01.001

[18] Gustafsson H, Isaksson S, Altskär A, Holmberg K. Mesoporous silica nanoparticles with controllable morphology prepared from oil-in-water emulsions. Journal of Colloid and Interface Science. 2016;**467**:253-260. DOI: 10.1016/j.jcis.2016.01.026

[19] Maity A, Polshettiwar V. Scalable and sustainable synthesis of size-controlled monodisperse dendritic fibrous nanosilica quantified by E-factor. ACS Applied Nano Materials. 2018;**1**:3636-3643. DOI: 10.1021/acsanm.8b00761

[20] Moon D-S, Lee J-K. Tunable synthesis of hierarchical mesoporous silica nanoparticles with radial wrinkle structure. Langmuir. 2012;**28**:12341-12347. DOI: 10.1021/la302145j

[21] Yu Y-J, Xing J-L, Pang J-L, Jiang S-H, Lam K-F, Yang T-Q, et al. Facile synthesis of size controllable dendritic mesoporous silica nanoparticles. ACS Applied Materials & Interfaces. 2014;**6**:22655-22665. DOI: 10.1021/am506653n

[22] Maity A, Polshettiwar V. Dendritic fibrous nanosilica for catalysis, energy harvesting, carbon dioxide mitigation, drug delivery, and sensing. ChemSusChem. 2017;**10**:3866-3913. DOI: 10.1002/cssc.201701076

[23] Singh R, Bapat R, Qin L, Feng H, Polshettiwar V. Atomic layer deposited (ALD) TiO_2 on fibrous nano-silica (KCC-1) for photocatalysis: Nanoparticle formation and size quantization effect. ACS Catalysis. 2016;**6**:2770-2784. DOI: 10.1021/acscatal.6b00418

[24] Schacht S, Huo Q, Voigt-Martin IG, Stucky GD, Schuth F. Oil-water interface templating of mesoporous macroscale structures. Science (80-.). 1996;**273**:768-771. DOI: 10.1126/science.273.5276.768

[25] Sanchez-Dominguez M, Pemartin K, Boutonnet M. Preparation of inorganic nanoparticles in oil-in-water microemulsions: A soft and versatile approach. Current Opinion in Colloid & Interface Science. 2012;**17**:297-305. DOI: 10.1016/j.cocis.2012.06.007

[26] Kuijk A, van Blaaderen A, Imhof A. Synthesis of monodisperse, rodlike silica colloids with tunable aspect ratio. Journal of the American Chemical Society. 2011;**133**:2346-2349. DOI: 10.1021/ja109524h

[27] Lind A, Spliethoff B, Lindén M. Unusual, vesicle-like patterned, mesoscopically ordered silica. Chemistry of Materials. 2003;**15**:813-818. DOI: 10.1021/cm021243o

[28] Wang S, Chen M, Wu L. One-step synthesis of cagelike hollow silica spheres with large through-holes for macromolecule delivery. ACS Applied Materials & Interfaces. 2016;**8**:33316-33325. DOI: 10.1021/acsami.6b11639

[29] Polshettiwar V, Cha D, Zhang X, Basset JM. High-surface-area silica nanospheres (KCC-1) with a fibrous morphology. Angewandte Chemie International Edition. 2010;**49**:9652-9656. DOI: 10.1002/anie.201003451

[30] ALOthman Z. A review: Fundamental aspects of silicate mesoporous materials. Materials (Basel). 2012;**5**:2874-2902. DOI: 10.3390/ma5122874

[31] Putz A-M, Cecilia S, Ianăşi C, Dudás Z, Székely KN, Plocek J, et al. Pore ordering in mesoporous matrices induced by different directing agents. Journal of Porous Materials. 2015;**22**:321-331. DOI: 10.1007/s10934-014-9899-z

[32] Moon D-S, Lee J-K. Formation of wrinkled silica mesostructures based on the phase behavior of pseudoternary systems. Langmuir. 2014;**30**:15574-15580. DOI: 10.1021/la504207k

[33] Rana S, Bhattacharjee J, Barick KC, Verma G, Hassan PA, Yakhmi JV. Interfacial engineering of nanoparticles for cancer therapeutics. In: Nanostructures Cancer Therapy. Amsterdam: Elsevier; 2017. pp. 177-209. DOI: 10.1016/B978-0-323-46144-3.00007-6

[34] Pileni MP. Reverse micelles as microreactors. The Journal of Physical Chemistry. 1993;**97**:6961-6973. DOI: 10.1021/j100129a008

[35] Danielsson I, Lindman B. The definition of microemulsion. Colloids and Surfaces. 1981;**3**:391-392. DOI: 10.1016/0166-6622(81)80064-9

[36] Aubery C, Solans C, Prevost S, Gradzielski M, Sanchez-Dominguez M. Microemulsions as reaction media for the synthesis of mixed oxide nanoparticles: Relationships between microemulsion structure, reactivity, and nanoparticle characteristics. Langmuir. 2013;**29**:1779-1789. DOI: 10.1021/la303817w

[37] Nič M, Jirát J, Košata B, Jenkins A, McNaught A, editors. IUPAC Compendium of Chemical Terminology. Research Triagle Park, NC: IUPAC; 2009. DOI: 10.1351/goldbook

[38] Hench LL, West JK. The sol-gel process. Chemical Reviews. 1990;**90**:33-72. DOI: 10.1021/cr00099a003

[39] Brinker CJ. Hydrolysis and condensation of silicates: Effects on structure. Journal of Non-Crystalline Solids. 1988;**100**:31-50. DOI: 10.1016/0022-3093(88)90005-1

[40] Febriyanti E, Suendo V, Mukti RR, Prasetyo A, Arifin AF, Akbar MA, et al. Ismunandar, further insight into the definite morphology and formation mechanism of mesoporous silica KCC-1. Langmuir. 2016;**32**:5802-5811. DOI: 10.1021/acs.langmuir.6b00675

[41] Maity A, Das A, Sen D, Mazumder S, Polshettiwar V. Unraveling the formation mechanism of dendritic fibrous nanosilica. Langmuir. 2017;**33**:13774-13782. DOI: 10.1021/acs.langmuir.7b02996

[42] Bayal N, Singh B, Singh R, Polshettiwar V. Size and fiber density controlled synthesis of fibrous nanosilica spheres (KCC-1). Scientific Reports. 2016;**6**:24888. DOI: 10.1038/srep24888

[43] Shen D, Yang J, Li X, Zhou L, Zhang R, Li W, et al. Biphase stratification approach to three-dimensional dendritic biodegradable mesoporous silica nanospheres. Nano Letters. 2014;**14**:923-932. DOI: 10.1021/nl404316v

[44] Yamada H, Urata C, Higashitamori S, Aoyama Y, Yamauchi Y, Kuroda K. Critical roles of cationic surfactants in the preparation of colloidal mesostructured silica nanoparticles: Control of mesostructure, particle size,

and dispersion. ACS Applied Materials & Interfaces. 2014;**6**:3491-3500. DOI: 10.1021/am405633r

[45] Yokoi T, Yoshitake H, Tatsumi T. Synthesis of amino-functionalized MCM-41 via direct co-condensation and post-synthesis grafting methods using mono-, di- and tri-amino-organoalkoxysilanes. Electronic supplementary information (ESI) available: XRD patterns of (A) x-dNN-MCM-41 and (B) x-dNNN. Journal of Materials Chemistry. 2004;**14**:951. DOI: 10.1039/b310576h

[46] Clark KG, Gaddy VL, Rist CE. Equilibria in the ammonium carbamate-urea-water system. Industrial and Engineering Chemistry. 1933;**25**:1092-1096. DOI: 10.1021/ie50286a008

[47] Jin H, Liu Z, Ohsuna T, Terasaki O, Inoue Y, Sakamoto K, et al. Control of morphology and helicity of chiral mesoporous silica. Advanced Materials. 2006;**18**:593-596. DOI: 10.1002/adma.200502038

[48] Hu Y, Martra G, Zhang J, Higashimoto S, Coluccia S, Anpo M. Characterization of the local structures of Ti-MCM-41 and their photocatalytic reactivity for the decomposition of NO into N_2 and O_2. The Journal of Physical Chemistry. B. 2006;**110**:1680-1685. DOI: 10.1021/jp058240u

[49] Li J, Zhou C, Xie H, Ge Z, Yuan L, Li X. Titanium-containing mesoporous materials: Synthesis and application in selective catalytic oxidation. Journal of Natural Gas Chemistry. 2006;**15**:164-177. DOI: 10.1016/S1003-9953(06)60023-6

[50] Livage J, Sanchez C. Sol-gel chemistry. Journal of Non-Crystalline Solids. 1992;**145**:11-19. DOI: 10.1016/S0022-3093(05)80422-3

[51] Angelomé PC, Andrini L, Calvo ME, Requejo FG, Bilmes SA, Soler-Illia GJAA. Mesoporous anatase TiO_2 films: Use of Ti K XANES for the quantification of the nanocrystalline character and substrate effects in the photocatalysis behavior. Journal of Physical Chemistry C. 2007;**111**:10886-10893. DOI: 10.1021/jp069020z

[52] Zhuravlev LT. Concentration of hydroxyl groups on the surface of amorphous silicas. Langmuir. 1987;**3**:316-318

[53] Kamegawa T, Yamashita H. Photocatalytic properties of TiO_2-loaded porous silica with hierarchical macroporous and mesoporous architectures. Nanostructures Science and Technology. Switzerland: Springer International Publishing; In: 2016: pp. 229-240. DOI: 10.1007/978-3-319-26079-2_13

[54] Ding Z, Lu GQ, Greenfield PF. Role of the crystallite phase of TiO_2 in heterogeneous photocatalysis for phenol oxidation in water. The Journal of Physical Chemistry. B. 2000;**104**:4815-4820. DOI: 10.1021/jp993819b

[55] Hanaor DAH, Sorrell CC. Review of the anatase to rutile phase transformation. Journal of Materials Science. 2011;**46**:855-874. DOI: 10.1007/s10853-010-5113-0

[56] Kundu S, Polshettiwar V. Hydrothermal crystallization of nano-titanium dioxide for enhanced photocatalytic hydrogen generation. ChemPhotoChem. 2018;**2**:796-800 (Copyright Wiley-VCH Verlag GmbH & Co. KGaA. Reproduced with permission. DOI: 10.1002/cptc.201800101